Author for correspondence:
Jyotisankar Ray,
Email: jsray65@hotmail.com

CAMBRIDGE
UNIVERSITY PRESS

Petrology of Palaeoarchaean mafic–ultramafic rock suites of the western Iron Ore Group, Singhbhum Craton, eastern India, using the chemistry of minerals

Madhuparna Paul[1], Jyotisankar Ray[1] , Christian Koeberl[2], Suresh C. Patel[3], Janisar M. Sheikh[3,4], C. Manikyamba[5], Moumita Gayen[1] and Nibedita Bhattacharjee[1]

[1]Department of Geology, University of Calcutta, Kolkata 700019, India; [2]Department of Lithospheric Research, University of Vienna, Althanstrasse 14, A-1090 Vienna, Austria; [3]Department of Earth Sciences, Indian Institute of Technology Bombay, Powai, Mumbai 400 076, India; [4]Department of Earth Sciences, Pondicherry University, Puducherry 605 014, India and [5]National Geophysical Research Institute (Council of Scientific and Industrial Research), Uppal Road, Hyderabad 500007, India

Abstract

The petrogenesis of Palaeoarchaean mafic–ultramafic rock suites from the western Iron Ore Group, Singhbhum Craton, eastern India, has been evaluated based on the chemistry of constituent mineral phases. The rock suites include basaltic rocks and mafic (gabbro) to ultramafic (serpentinized peridotite) intrusive rocks, which occur in host rocks covering phyllite, ferruginous shale, banded haematite quartzite and jasper. The constituent clinopyroxene shows dominant uralitization, whereas plagioclase grains are generally saussuritized, being marked by relatively tiny granular aggregates of albite, chlorite, epidote and K-feldspar. The ultramafic intrusive rocks are overwhelmingly serpentinized. Clinopyroxene compositions are augitic, whereas relict plagioclase is typically bytownite. Amphiboles of the investigated rock suites are divisible into the 'uralite' type (occurring peripherally to clinopyroxene) and the 'completely changed-over amphibole' type (with no traces of initial clinopyroxene). Both the amphibole types belong to the 'calcic group', showing a compositional spectrum from actinolite–magnesiohornblende–ferrohornblende–ferroactinolite. Opaque minerals include magnetite (both Cr-magnetite and Al-magnetite), chromite (Al-chromite) and ilmenite, whereas serpentine (belonging to the ultramafic intrusive rocks) corresponds to lizardite. Looking at the mineral compositions of the pyroxene, glass and amphibole, the studied rock suites show a wide equilibration temperature–pressure domain range (~750 °C to ~1400 °C at ~0.26 kbar to ~21 kbar), which corresponds to an ascending magma that underwent a 'hydration event' at a shallow level. The assessment of the clinopyroxene and spinel chemistry characteristically suggests an arc setting for the parent magma that has undergone both equilibrium and fractional crystallization in the course of magmatic evolution. During differentiation, the magmatic density remains almost constant, with variable oxygen fugacity.

1. Introduction

The assessment of the mineral chemistry of constituent phases plays an important role as a petrogenetic indicator for mafic–ultramafic rock suites (Friend *et al.* 2002; Malviya *et al.* 2006; Pettigrew & Hattori, 2006; Guice *et al.* 2018; Ali *et al.* 2021; Abdelfadil *et al.* 2022). Palaeoarchaean mafic–ultramafic assemblages were subjected to multiple deformation and metamorphic episodes and, in most instances, the primary mineralogy is beyond recognition (Polat & Hofmann, 2003; Byerly & Lowe, 2014). Although data are scant for such Palaeoarchaean rocks, some crucial sets of information have been recorded from several parts of the world where mineral chemistry could play an important role in evaluating the petrogenesis of mafic–ultramafic rock suites. The Palaeoarchaean abyssal peridotites from the Itsaq Gneiss Complex (>3800 Ma) of Southern West Greenland (Friend *et al.* 2002) record massive dunites and harzburgites, with those rocks bearing both spinel-bearing and garnet-free assemblages that indicate an equilibration pressure below ~20 kbar and a temperature above ~800 °C (O'Neill, 1981; Schmädicke, 2000; Friend *et al.* 2002). For Archaean mafic–ultramafic rocks from the Mauranipur supracrustal rocks of the Bundelkhand Craton, India, and the Ben Strome Complex of Scotland, the spinel chemistry has been successfully used to discern the distinct petrogenesis and tectonic setting (Malviya *et al.* 2006; Guice *et al.* 2018). The Ben Strome Complex has been ascribed to have a 'layered intrusion affinity' based on spinel chemistry (Guice *et al.* 2018). Spinel chemistry has been found to be effective for evaluating the

petrotectonic setting of the host rocks (Barnes & Roeder, 2001; Malviya *et al.* 2006). Clinopyroxene compositions mostly involving SiO$_2$, Al$_2$O$_3$, TiO$_2$ and Al$_z$ in atoms per formula unit (apfu) (where Al$_z$ = 100 × ^{IV}Al/2) were successfully employed to discriminate the arc signature for the Quetico Intrusions of the Western Superior Province and were attributable to the Neoarchaean Alaskan/Ural-type zoned mafic–ultramafic intrusions (Pettigrew & Hattori, 2006). In the global scenario for Palaeoarchaean mafic–ultramafic rock suites, the attempt to elucidate petrogenetic aspects using mineral chemistry is rather rare. In order to decipher the style of early crustal growth in the eastern Indian shield, we have investigated Palaeoarchaean mafic–ultramafic rocks (~3392 to ~3507 Ma; Basu *et al.* 2008; Mukhopadhyay *et al.* 2008) of the western Iron Ore Group of the Singhbhum Craton based on mineral chemistry. The availability of such deduced petrogenetic data would give us an idea of the nature of magma evolution during the formation of proto-crust globally.

2. Geological background

The Precambrian geological history of Peninsular India covers nearly three billion years of time, and it involves a complex geological evolutionary history (Meert *et al.* 2010). In this situation, some important geological documentation (related to the complex evolutionary history of the Indian Plate and the Singhbhum Craton in particular) has been described in a brief manner. The stable configuration of the Indian Plate was completed by 2.5 Ga (Radhakrishna & Naqvi, 1986), where the role of the Indian Plate in various supercontinental cycles has been highlighted by several workers (Rogers & Santosh, 2002; Veevers, 2004; Li *et al.* 2008). The general consensus of opinion is that the Indian cratonic nuclei are constituted by tonalite–trondhjemite–granodiorite gneisses (TTGs), greenstone enclaves and Archaean supracrustal rocks, which were invaded later by potassic granites (Misra *et al.* 1999; Jayananda *et al.* 2008; Ramakrishnan & Vaidyanadhan, 2008). For the Singhbhum Craton of Peninsular India, the following important points are to be noted: (i) the Singhbhum Craton covers an area of ~39 000 km^2 and forms a N–S elongate ovoid block lying between 84.5 °E to 86.5 °E and 21 °N to 22.75 °N in eastern India. This craton also embraces different rock units ranging in age from 3.5 to 2.5 Ga (Mukhopadhyay, 2001; Matin *et al.* 2012; Sarkar & Gupta, 2012; Mukhopadhyay & Matin, 2020); (ii) The North Singhbhum Mobile Belt is thrust over the Singhbhum Craton along the arcuate Singhbhum Shear Zone, where the Singhbhum Shear Zone has a history of reactivation multiple times; (iii) The stratigraphic succession of the Singhbhum–Orissa Craton has been reported by Saha *et al.* (1988) and Misra (2006) (Table 1); (iv) This stratigraphic succession has scope for further modification considering the availability of geochronological data (Mukhopadhyay & Matin, 2020 and recent studies by other workers; see Table 1); (v) The Iron Ore Group (IOG) basin as a whole comprises three principal sub-parts which are: the western IOG belt (Noamundi–Jamda–Koira basin), eastern IOG belt (Gorumahisani–Badampahar basin) and southern IOG belt (Tomka–Daitari basin) (Fig. 1); (vi) Some important geochronological data for the western IOG include an age of 3392 ± 29 Ma (Basu *et al.* 2008). For the southern IOG, geochronological data reveals ages of 3507 ± 2 Ma (Mukhopadhyay *et al.* 2008) and 3505 ± 5 Ma (Sreenivas *et al.* 2019). For the eastern IOG, an indirect age of 3.1 Ga has been inferred by Saha (1994), though some recent geochronological input is available in the literature and those have been cited in Table 1 (Nelson *et al.* 2014;

Olierook *et al.* 2019; Hofmann *et al.* 2022). The present study area (belonging to the western IOG), therefore, in all probability corresponds to a Palaeoarchaean age (Sarkar & Gupta, 2012; Paul *et al.* 2021; Mahapatra *et al.* 2022).

3. Field geology

The study area was divided (and systematically studied) into the following sectors: (a) the Koira sector, (b) the Gua–Manoharpur sector and (c) the Sahedba–Santara sector (Fig. 1). The rock units (encompassing all three sectors) are divisible into the following types: (i) highly schistose phyllite and ferruginous shale (more dominant) with a local presence of primary compositional layers; (ii) banded iron formation (BIF) comprising banded haematite quartzite and banded haematite jasper; and (iii) basaltic rocks and mafic (gabbro) – ultramafic (peridotite) intrusive rocks (Fig. 2a–c). A comprehensive litholog showing the height-wise distribution of different lithologies has been carefully prepared based on the present study, and its geological implications have been shown in Figure 2d. Figure 3a–h shows representative field photographs of different lithologies of the investigated area, which depict the field characteristics and spatial interrelationships of the different lithounits.

4. Petrography of basalts and intrusive rocks

In hand specimen, the basaltic rocks are mesocratic, merocrystalline and inequigranular. The gabbroic rocks, on the other hand are meso-melanocratic, coarse grained and inequigranular. The ultramafic intrusive rocks (peridotite) in hand specimen show a dominantly serpentinized nature. Microscopic study of these rocks (basalts–gabbro–ultramafic) reveals that their essential mineralogies show a change-over to secondary minerals. For instance, in samples of both basalts and gabbro, primary clinopyroxene has often been altered to uralite, and initial plagioclase shows the effects of saussuritization (where granular aggregates of albite, chlorite, epidote and K-feldspar have been noted). In both cases (for basalt–gabbro), however, relict primary mineralogy and relict textures (namely ophitic, sub-ophitic and intergranular) have been recorded. The ultramafic intrusive rocks, under the microscope, have a mesh-like appearance defined by the constituent minerals. In the ultramafic type, euhedral/subhedral opaque crystals and minute dolomite grains (pseudomorphs after olivine) have been observed. Representative photomicrographs of these rock types have been presented in Figure 4a–h.

5. Mineral chemistry

The electron probe microanalysis (EPMA) data for different constituent minerals of the basalt–gabbro–ultramafic association were determined using a CAMECA SX-5 electron probe micro analyser at the Department of Earth Sciences, Indian Institute of Technology (IIT) Bombay, India. The analytical conditions for the instrument involved an acceleration voltage of 15 kV, a beam current of 20 nA and a nominal beam diameter of 3 μm. Both natural and synthetic standards were used for calibration of the elements and data correction was done using the X-PHI method.

Pyroxene. EPMA data for the pyroxenes are available in online Supplementary Material Table S1. Species level classification indicates that the pyroxene belongs to augite (Morimoto, 1989; Fig. 5a).

Table 1. Stratigraphy of the Singhbhum–Orissa Craton, eastern India. After Saha *et al.* (1988) and Misra (2006)

Stratigraphic unit	Geological events	Major lithologies	Age (Ga) (by Misra, 2006)	Updated age (Ga) (references are within parentheses)
Newer dolerite dykes and sills – phases I, II and III	Intrusions of dykes and sills	Quartz dolerite	~2.0–1.0	2.26 (Srivastava *et al.* 2019)
Kolhan group	Deposition of sediments	Phyllite, limestone, sandstone-conglomerate	~<2.25	
Jagannathpur and Malangtoli lavas	Volcanic eruption	Basalts, basaltic andesites	~2.25	2.8 (Adhikari *et al.* 2021)
Dhanjori and Dalma volcanics; Tamperkola granites	Mafic volcanism and felsic plutonism	Ultramafic–mafic tuffs, basalts, quartzite-conglomerate; High Mg-lavas, pyroclastic rocks, granite	~2.80	3.33 (Acharyya *et al.* 2010)
Thermal metamorphism of OMG, OMTG, SBG-II and SBG-III			3.07–3.05	
Mayurbhanj granite and gabbro	Coeval emplacement of MBG	Granite, gabbro, picrate, anorthosite	3.09	3.09 (Chakraborti *et al.* 2019)
Simlipal lavas and metasediments	Formation of volcano-sedimentary basin	Spillites, tuffs, quartzites	~>3.09	3.08 (Bhattacharjee *et al.* 2021)
Singhbhum Group	Formation and deformation of supracrustal rocks; sedimentation and magmatism	Pelites, felsic volcanic, mafic sills	~3.12–3.09	
Unconformity				
Thermal metamorphism of OMG due to SBG-III and Bonai granite emplacement			~3.16–3.10	
SBG-III	Emplacement of SBG-III	Granodiorite, granite	~3.12	3.38 (Chaudhuri *et al.* 2018
Bonai granite	Plutonic emplacement	Granite, granodiorite	~3.16	3.37 (Chakraborti *et al.* 2019)
Metamorphism of OMG, OMTG and IOG rocks			~3.24–3.20	
Iron Ore Group	Formation, structural deformation (folding) and metamorphism of IOG rocks	Mafic and felsic lavas, tuffs, shales, BHJ, BHQ, quartzite, dolomite, conglomerate	~3.30–3.16	WIOG – 3.4 (Basu *et al.* 2008) & 3.05 (Adhikari & Vadlamani, 2022); SIOG – 3.5 (Mukhopadhyay *et al.* 2008); EIOG – 3.33 (Nelson *et al.* 2014)
Unconformity				
Thermal metamorphism of OMG and OMTG due to SBG-II and Nilgiri granite emplacement			~3.30	
Nilgiri granite	Emplacement of Nilgiri granite	Tonalite, granite	~3.29	
SBG-II	Emplacement of SBG-II	Granodiorite	~3.33–3.30	3.34 (Upadhyay *et al.* 2014)
Singhbhum granite (SBG-I)	Emplacement of granitoid plutons	Tonalite, granodiorite	~3.44–~3.38	3.4 (Chaudhuri *et al.* 2018)
Older Metamorphic Tonalite Gneiss	Folding of OMG supracrustals and synkinematic intrusion of tonalite	Tonalite gneiss, granodiorite	~3.44–3.42	3.44 (Upadhyay *et al.* 2014)
Older Metamorphic Group	Deposition of sediments with mafic volcanism and plutonism	Pelitic schists, banded calc-gneiss, amphibolites	~3.55–3.44	3.37 (Nelson *et al.* 2014)
Unstable sialic crust		Sialic sediments	3.6–~3.55	

BHJ – banded haematite jasper; BHQ – banded haematite quartzite; EIOG – eastern Iron Ore Group; IOG – Iron Ore Group; MBG – Mayurbhanj granite and gabbro; OMG – Older Metamorphic Group; OMTG – Older Metamorphic Tonalite Gneiss; SBG-I, -II, -III – Singhbhum Granite I, II and III; SIOG – southern Iron Ore Group; WIOG – western Iron Ore Group.
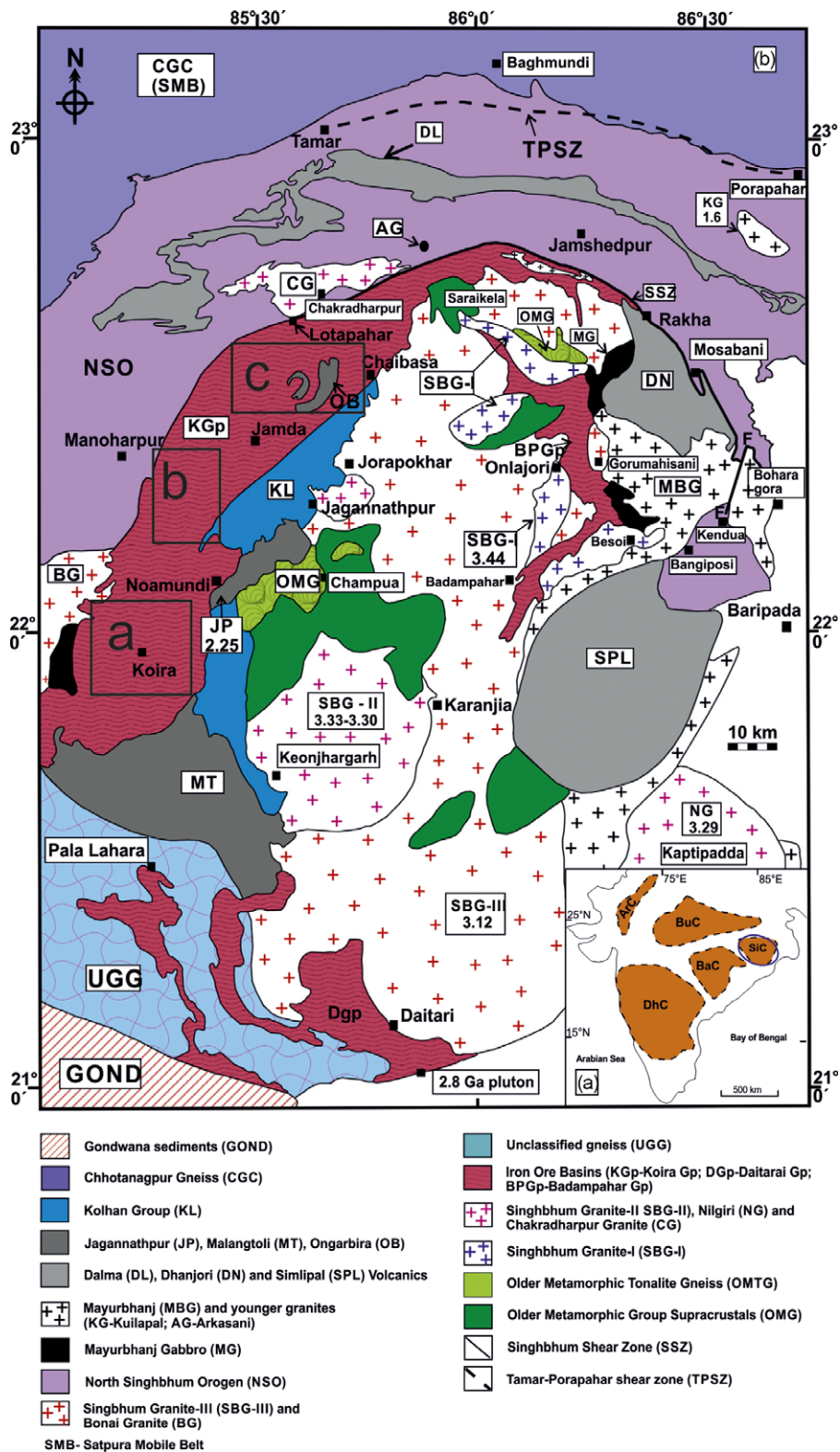
Fig. 1. (Colour online) Regional map showing disposition of several rock units in the Singhbhum North Orissa region, eastern India (after Saha, 1994; Misra, 2006; Singh *et al.* 2016); marked areas represent investigated sectors: a – Koira sector, b – Gua–Manoharpur sector and c – Sahedba–Santara sector. Inset map shows distribution of different cratons in the Peninsular India (Sharma, 2009); DhC – Dharwar Craton; BaC – Bastar Craton; SiC – Singhbhum Craton; BuC – Bundelkhand Craton; ArC – Aravalli Craton.
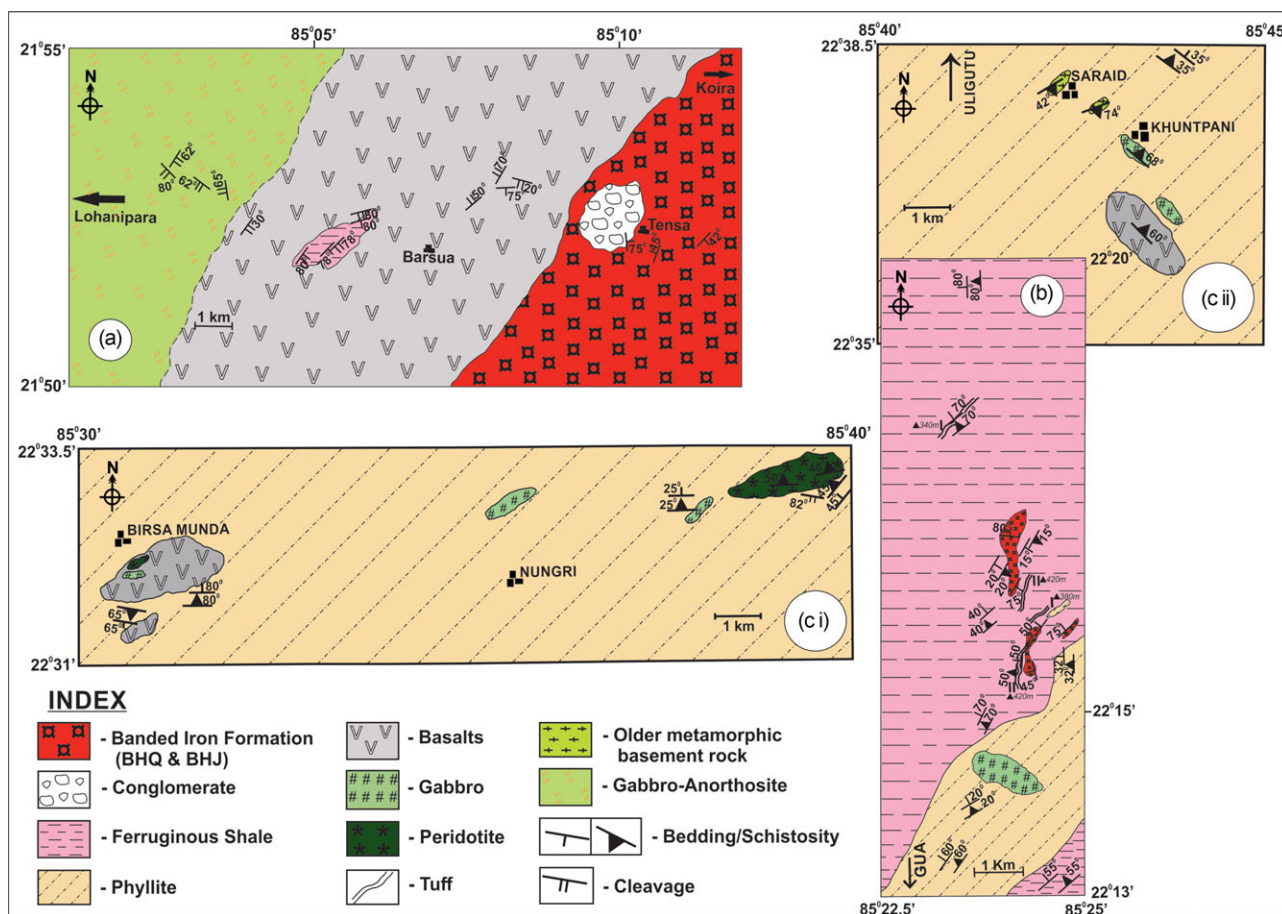
Fig. 2. (Colour online) Geological map (prepared by the present authors) of the study areas corresponding to the different sectors: (a) Koira sector, (b) Gua–Manoharpur sector and (c) Sahedba–Santara sector (see Fig. 1). The geological map corresponding to sector (c) has been shown in terms of (i) and (ii) for easy understanding of the different lithological units. (d) Litholog (prepared by the present authors) showing the distribution of different lithologies of the study area.

Plagioclase. EPMA data for the plagioclase compositions are given in online Supplementary Material Table S2. Plagioclase grains in the basalt and gabbro are hydrothermally altered and changed to albite or oligoclase. Relict plagioclase grains are mostly bytownite (Fig. 5b).

Amphibole. The amphibole may be divided into two distinct types, namely, (i) uralite occurring peripherally to clinopyroxene and (ii) completely changed-over amphibole with no traces of initial pyroxene. EPMA data for these two types of amphiboles are given in online Supplementary Material Table S3. The amphibole compositions in the classification scheme of Leake (1978) and Leake *et al.* (1997) are found to be 'calcic' (Fig. 5c), and the species level classification diagram ($Mg/(Mg + Fe_2)$ versus TSi) further shows a compositional spectrum from actinolite–magnesiohornblende–ferrohornblende and ferroactinolite (Hawthorne *et al.* 2012; Fig. 5d).

Opaque minerals and serpentine. Opaque minerals in this study are of three types, which include magnetite, chromite and ilmenite. The EPMA data for these opaque phases are available in online Supplementary Material Tables S4–S6. The Fe^{3+}–Cr–Al diagram (Stevens, 1944; Fig. 6a) suggests that the magnetite belongs to both the Cr-magnetite and Al-magnetite variants, while the chromite composition belongs to the Al-chromite field. Serpentine occurs in the peridotite, and its EPMA data are available in online Supplementary Material Table S7. The Si–Mg + Fe–Ni diagram

(after Villanova-de-Benavent *et al.* 2014; Fig. 6b) shows that the serpentine corresponds to the lizardite variety.

Other phases. Other phases include chlorite, epidote, K-feldspar and titanite. The EPMA data for chlorite are available in online Supplementary Material Table S8. The classification diagram based on $Fe_2 + Fe_3$ versus Si (Hey, 1954) suggests that the chlorite species belong to pycnochlorite and brunsvigite; rare spillovers to diabantite and ripidolite have also been observed (Fig. 6c). The EPMA data for epidote, K-feldspar and titanite are given in online Supplementary Material Tables S9, S10 and S11, respectively.

6. Geothermobarometry

Thermobarometric evaluation of mafic rocks (with low-grade reconstitution) using suitable mineral chemical data was attempted by Putirka (2008) and Ridolfi *et al.* (2010). With this background, in the present study, the chemistry of the constituent minerals such as clinopyroxene and amphibole has been used to decipher the nature of temperature and pressure equilibration.

6.a. Geothermometry

Thermometric data for clinopyroxene and glass (~parent melt) were evaluated using the method of Putirka (2008), and their
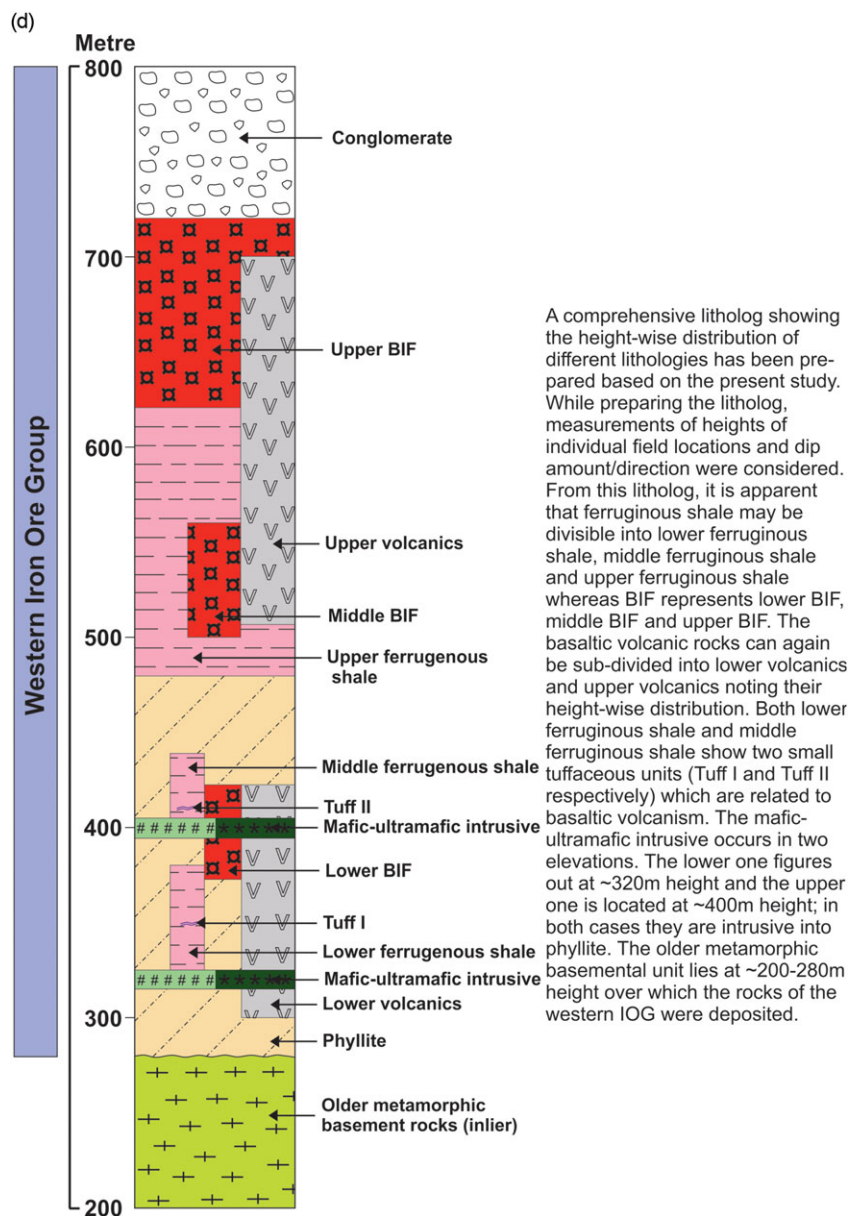
(d)

A comprehensive litholog showing the height-wise distribution of different lithologies has been prepared based on the present study. While preparing the litholog, measurements of heights of individual field locations and dip amount/direction were considered. From this litholog, it is apparent that ferruginous shale may be divisible into lower ferruginous shale, middle ferruginous shale and upper ferruginous shale whereas BIF represents lower BIF, middle BIF and upper BIF. The basaltic volcanic rocks can again be sub-divided into lower volcanics and upper volcanics noting their height-wise distribution. Both lower ferruginous shale and middle ferruginous shale show two small tuffaceous units (Tuff I and Tuff II respectively) which are related to basaltic volcanism. The mafic-ultramafic intrusive occurs in two elevations. The lower one figures out at ~320m height and the upper one is located at ~400m height; in both cases they are intrusive into phyllite. The older metamorphic basemental unit lies at ~200-280m height over which the rocks of the western IOG were deposited.

Fig. 2. (Continued)

corresponding temperatures are presented in Table 2. From this table, it is clear that the equilibration temperatures (after Putirka, 2008) reveal an overall range from ~1100 °C to ~1400 °C. For the different rock specimens, the glass and pyroxene thermometry reveal almost similar values; this may suggest pyroxene corresponds to an early part of the crystallization history.

We noted earlier (see Section 4) that most of the constituent clinopyroxene grains have been altered to amphibole (uralite) under hydrothermal conditions. Even so, the determination of pressure–temperature conditions of the mafic rocks with the help of those amphibole data (Table 3) is quite encouraging (Ridolfi *et al.* 2010; Ridolfi & Renzulli, 2012; Zhang *et al.* 2017). Plots for amphibole compositions when referred to the pressure–temperature variational grid pattern (Fig. 7a) (Ridolfi *et al.* 2010) suggest a temperature equilibration range of ~750 °C to ~850 °C with an almost near-surficial pressure (~0.5 kbar). Figure 7b suggests a variation of log fO_2 versus T °C, which indicates an oxygen fugacity range from −11 to −14 units. This suggests that oxygen fugacity

varied within the magma chamber during crystallization and subsequent hydration (Ridolfi *et al.* 2010). The presence of H_2O (wt %) in the ambient melt (during hydration) and the relevant temperature can be bracketed using a T °C versus H_2O_{melt} (wt %) diagram (Fig. 7c). All the data plots for this study characteristically occupy the amphibole stability field.

6.b. Geobarometry

Geobarometry can be assessed using the compositions of clinopyroxene (Table 2; Putirka, 2008). From the table, the following observations can be made: (i) one gabbro sample (sample no. 1004) reveals two equilibration pressure levels at ~16 to ~18 kbar and ~3 to ~6 kbar, whereas another gabbro sample (sample no. 994a) reveals a ~15 to ~21 kbar equilibration pressure, and (ii) the basaltic rock (sample no. 840) indicates an equilibration pressure range corresponding to ~15 to ~21 kbar. It is possible that the mafic magma experienced equilibration under a range of pressures,
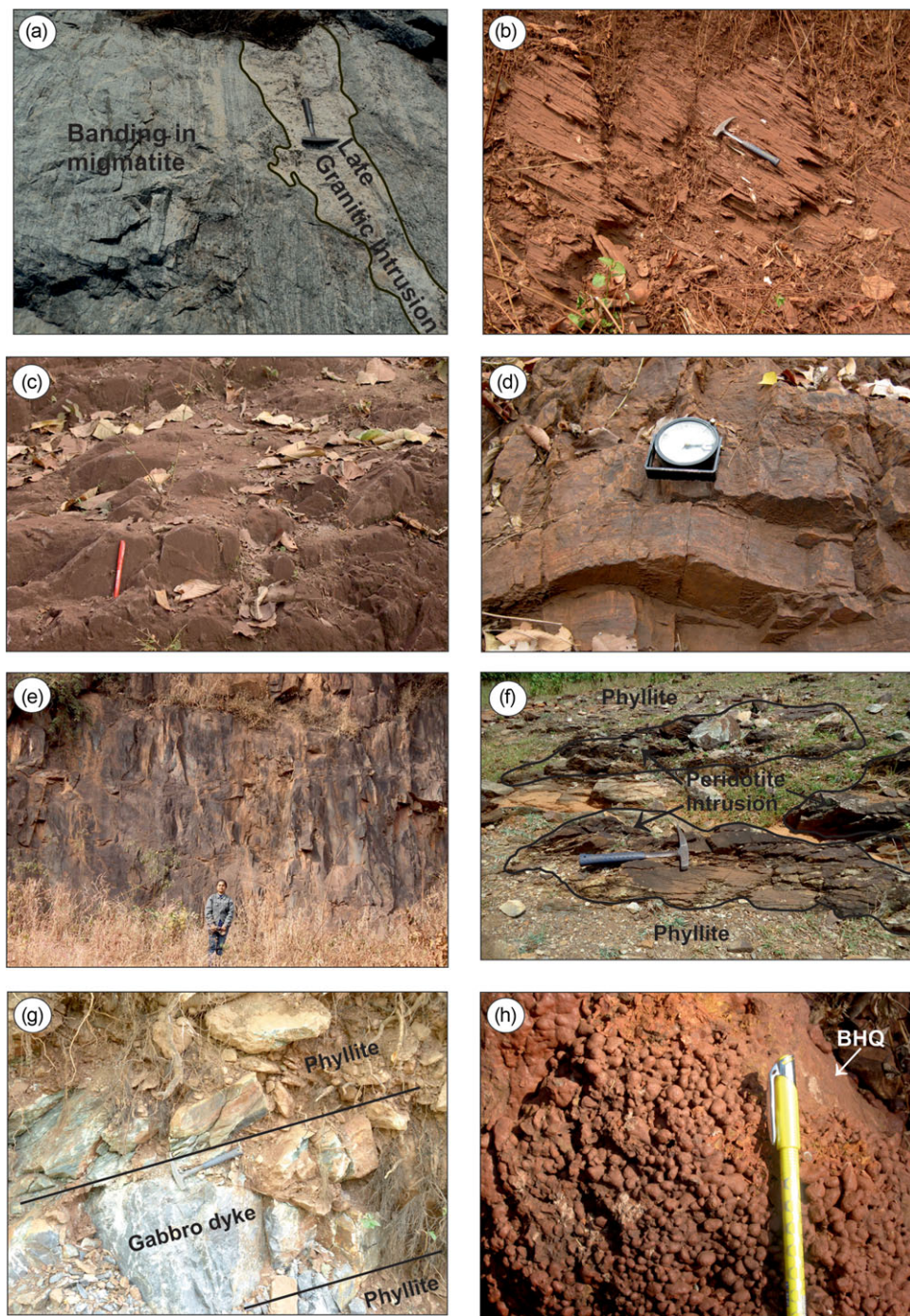
Fig. 3. (Colour online) Field photograph showing (a) exposure of basemental older metamorphic migmatitic gneiss traversed by a granitic intrusion; (b) a sectional view of phyllite showing prominent schistosity; (c) ferruginous shale with a nearly vertical attitude of schistosity plane; (d) an exposure of banded haematite jasper (BHJ) showing open folding with a nearly sub-horizontal axis; (e) well-developed columnar jointing pattern in basaltic rock; (f) a peridotite lensoidal intrusion into phyllite; (g) exposure of a gabbro dyke invading the adjacent phyllitic rock; (h) a local patch of conglomerate spatially associated with banded haematite quartzite (BHQ).

i.e. ~21 to ~3 kbar, which corresponds to magma storage (and crystallization) at an upper mantle depth followed by relatively near-surface crystallization (~3 to ~6 kbar) due to ascent.

Since pyroxene altering to amphibole is common in mafic rocks (Stakes & Vanko, 1986; Gillis, 1995) corresponding to hydrothermal events, Ridolfi *et al.* (2010) presented a unique method of pressure calculation. In the investigated cases (where clinopyroxene is dominantly converted to amphibole), the pressure evaluated through Ridolfi's method has been furnished in Table 3. From this table, it is apparent that the pressure (corresponding to hydration environments) ranges from 0.26 to 0.35 kbar. It is, therefore, evident that the hydration event is a near-surficial condition that was imposed upon the original magma crystallization episode.
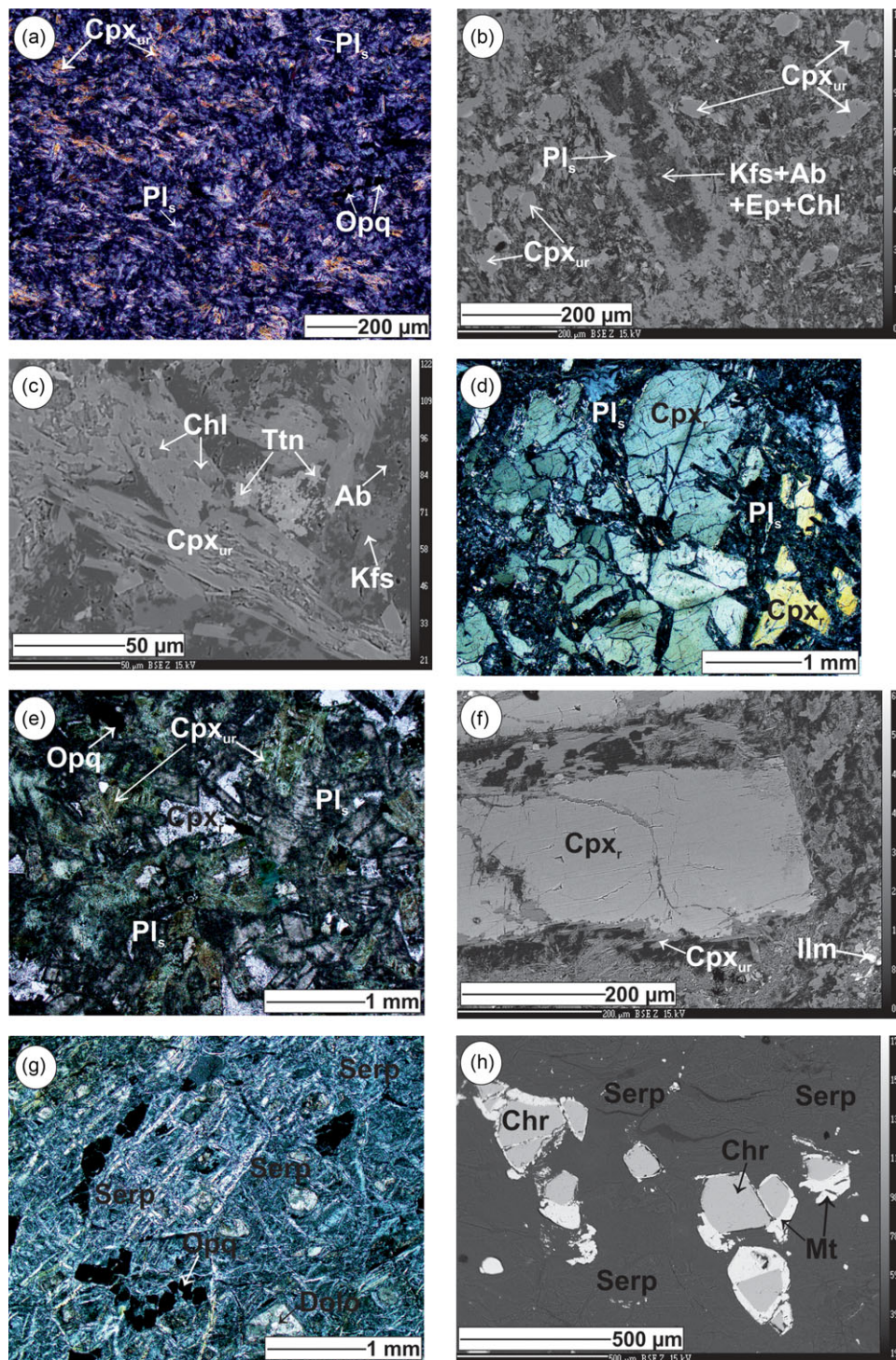
Fig. 4. (Colour online) (a) Photomicrograph of basalt from the Koira sector showing the dominant presence of uralitized clinopyroxene (Cpx$_{ur}$) and saussuritized plagio-clase (Pl$_s$). Small euhedral opaque grains (Opq) are also present. (b) Back-scattered electron (BSE) image of basaltic rocks of the Koira sector showing the presence of a large saussuritized plagioclase (Pl$_s$) phenocryst. The plagioclase phenocryst is charged with numerous secondarily formed minerals such as albite (Ab), epidote (Ep), chlorite (Chl) and K-feldspar (Kfs). Prismatic uralitized clinopyroxene grains (Cpx$_{ur}$) have also been noticed. (c) BSE image of basaltic rocks of the Koira sector showing the presence of a prismatic uralitized clinopyroxene grain (Cpx$_{ur}$) which is often broken down to chlorite (Chl). The margin of the image shows an elongated plagioclase grain with albite (Ab) and K-feldspar (Kfs) change-over. Some titanite (Ttn) is also present. (d) Photomicrograph of a gabbroic intrusive from the Gua–Manoharpur area showing a characteristic relict prismatic grain of clinopyroxene (Cpx$_r$) which encloses saussuritized plagioclase (Pl$_s$) ophitically and sub-ophitically. (e) Photomicrograph of gabbroic rock from the Sahedba–Santara sector showing relict clinopyroxene (Cpx$_r$), saussuritized plagioclase (Pl$_s$) and euhedral opaque grains (Opq). Some of the clinopyroxene grains have been uralitized (Cpx$_{ur}$). Overall, the rock shows a hypidiomorphic granular texture. (f) BSE image of a gabbroic rock from the Gua–Manoharpur area showing a large phenocryst of relict clinopyroxene (Cpx$_r$) which shows both marginal and fracture controlled uralitization (Cpx$_{ur}$). Small ilmenite grain (Ilm) is present as an accessory. (g) Photomicrograph of a representative peridotite intrusive from the Sahedba–Santara sector showing the overwhelming presence of serpentine (Serp) giving rise to a mesh-like pattern. Euhedral to subhedral opaque grains (Opq) and dolomite (Dolo) are also present. (h) BSE image of a peridotite intrusive from the Sahedba–Santara area showing the characteristic presence of overwhelming serpentine (Serp) and chromite–magnetite (Chr–Mt) intergrowth.
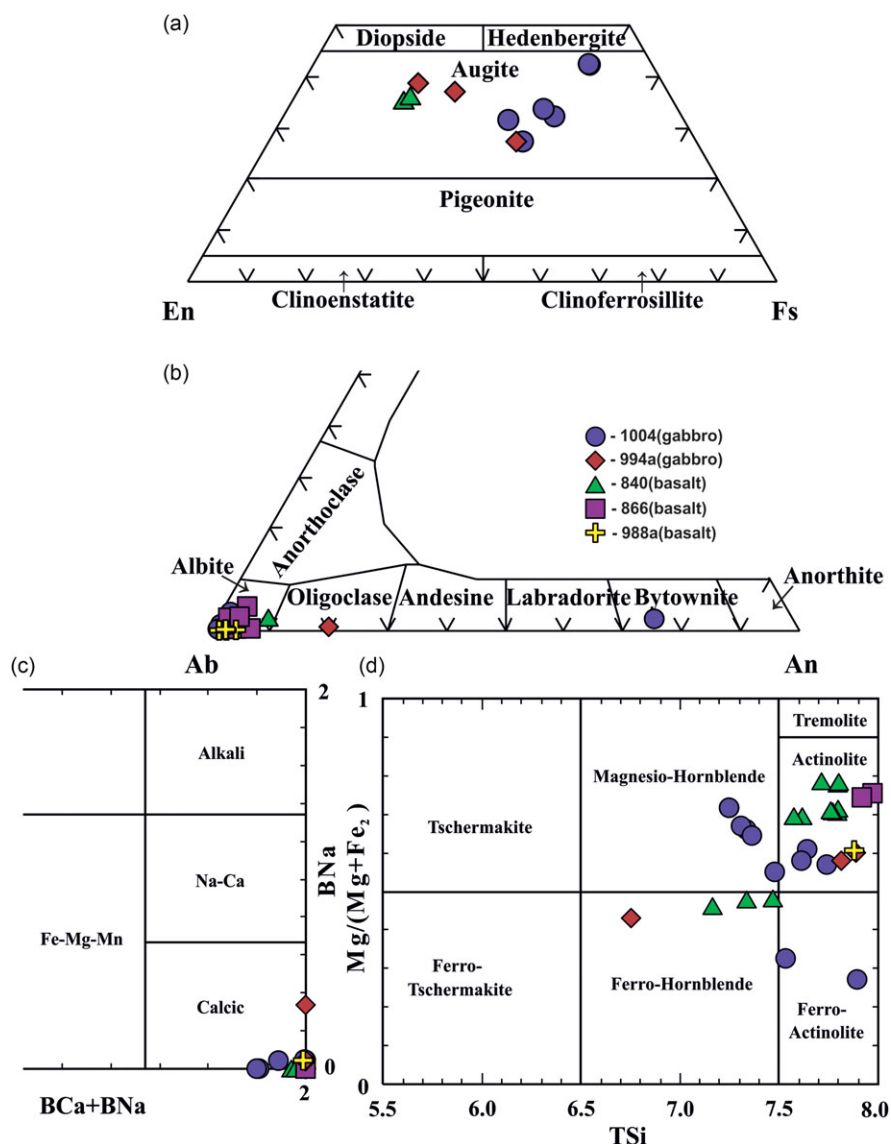
Fig. 5. (Colour online) Plots of investigated minerals from different lithologies of the present study: (a) Classification diagrams for pyroxene (Morimoto *et al.* 1988; Morimoto, 1989). (b) Classification diagram for plagioclase. (c, d) Classification diagrams for amphibole (Leake *et al.* 1997; Hawthorne *et al.* 2012). Note: In the majority of the cases, the plagioclase composition of the gabbros/basalts have been re-equilibrated to albite/oligoclase (only the relict plagioclase composition corresponding to the bytownite field has been recorded); for details see text.

7. Discussion

7.a. Melt composition and hydration event

Clinopyroxene compositions have often been used to constrain the parental composition of mafic igneous rocks (Leterrier *et al.* 1982; Loucks, 1990; Das *et al.* 2020). Therefore, in the present research, (relict) clinopyroxene chemistry has been used as a potential assessor to understand the nature of the parental magma. The tholeiitic/ sub-alkaline character of the parent-melt composition has also been depicted in Figure 8a (Leterrier *et al.* 1982), which involves a variation pattern of Ti (pfu) versus Ca + Na (pfu). Figure 8b depicts the interrelationship between Al$_z$ versus TiO$_2$ (wt %) in Cpx where a broad arc-related affinity (Loucks, 1990) for the parent melt has been suggested.

The nature of the ambient conditions of amphibole formation and its stability has been established by several workers in recent years (Ridolfi *et al.* 2010; Ridolfi & Renzulli, 2012; Zhang *et al.* 2017). It has been earlier deduced that for the present rocks, hydration events represent a near-surface (secondary) phenomenon, with progressive ingress of water into the magma chamber. As a

result, the original magmatic temperature has been substantially reduced, and in the presence of water, such temperatures have been recalibrated to the range of ~750 °C to ~850 °C (deduced using the method of Ridolfi *et al.* 2010) (Table 3). In this context, it would be worthwhile to assess the changed magma composition after hydration. The calibrated melt composition (corresponding to a hydration event) can be critically calculated based on equations proposed by Zhang *et al.* (2017). The effects of hydration on several oxides such as SiO$_2$, Al$_2$O$_3$, TiO$_2$, MgO, CaO and K$_2$O have been depicted in Figure 9. This figure suggests that SiO$_2$, Al$_2$O$_3$ and K$_2$O increase after hydration whereas TiO$_2$, MgO and CaO decrease with hydration. These elevating and declining major oxide patterns (as stated above) can mainly be ascribed to the alteration of pyroxene to amphibole (Deer *et al.* 1992).

The plagioclase compositions of the mafic rocks fall mainly in the sodic plagioclase field (albite–oligoclase) of the Or–Ab–An classification (Fig. 5b). However, the plagioclase composition from the gabbroic rock occasionally retains its relict character where the composition corresponds to bytownite (Fig. 5b). It is, therefore,

**Table 2.** Thermobarometry data using pyroxene* and glass compositions (after Putirka, 2008)

Sample no.	Locality/sector	Rock type	Pyroxene thermometry (°C)	Pyroxene barometry (kbar)	Glass thermometry† (°C)
1004	Gua–Manoharpur	Gabbro	1065–1302	2.8–6.4 16.6–17.6	1179
994a	Sahedba–Santara	Gabbro	1266–1433	15.1–20.4	1322
840	Koira	Basalt	1256–1334	14.9–21.4	1226

*During calculation, pyroxene grains lying in close proximity to epidote were not considered.
†Calculations involved unpublished whole-rock major element data of M. Paul (first author of this paper).

Table 3. Thermobarometry data of amphibole after Ridolfi *et al.* (2010)

| Sample no.	Locality/sector	Rock type	Temperature estimation (°C)	Pressure estimation (kbar)	H_2O in melt (wt %)	fO_2	ΔNNO
1004	Gua–Manoharpur	Gabbro	778–837	0.26–0.31	5.2–6.8	11.6–13.8	0.4–1.5
840	Koira	Basalt	777–804	0.27–0.35	5.0–5.8	11.6–12.7	1.5–2.2
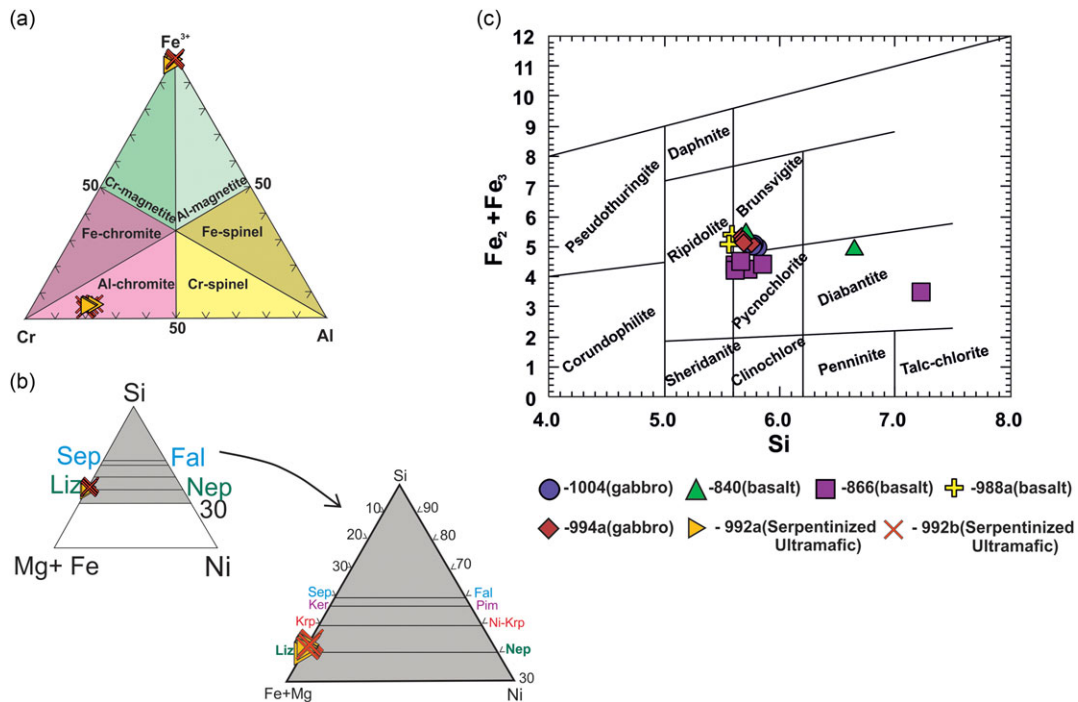
Fig. 6. (Colour online) Plots of investigated minerals for classification: (a) spinel (Stevens, 1944); (b) serpentine (Villanova-de-Benavent *et al.* 2014); (c) chlorite (Hey, 1954). Note: Opaque minerals are classified as Al-chromite, and Cr-magnetite and Al-magnetite.

evident that the majority of the initially formed calcic plagioclase has been re-equilibrated to albite and oligoclase, corresponding to a shallower depth (2–3 kbar) (online Supplementary Material Table S2). It appears, therefore, that the latter hydration event has also affected the initial plagioclase chemistry. According to Hövelmann *et al.* (2010), a pressure–temperature domain in the range of 600 °C and 2 kbar in an aqueous sodium silicate environment can substantially modify calcic plagioclase (labradorite) to albite–oligoclase. This further indicates an interface-coupled dissolution–reprecipitation mechanism. Such a mineralogical

transformation from calcic plagioclase to sodic plagioclase also involves the development of actinolite, chlorite and epidote assemblages (Humphris & Thompson, 1978). Thus, the recorded mineralogical assemblages in the present study (relict pyroxene – actinolitic hornblende – albitic plagioclase – chlorite – epidote) clearly correspond to relatively low-temperature hydration events aided by sodium in the aqueous solution (Stünitz & Tullis, 2001; Marti *et al.* 2018).

The ultramafic intrusive rocks in the study area are very serpentinized. The process of serpentinization is very dominant
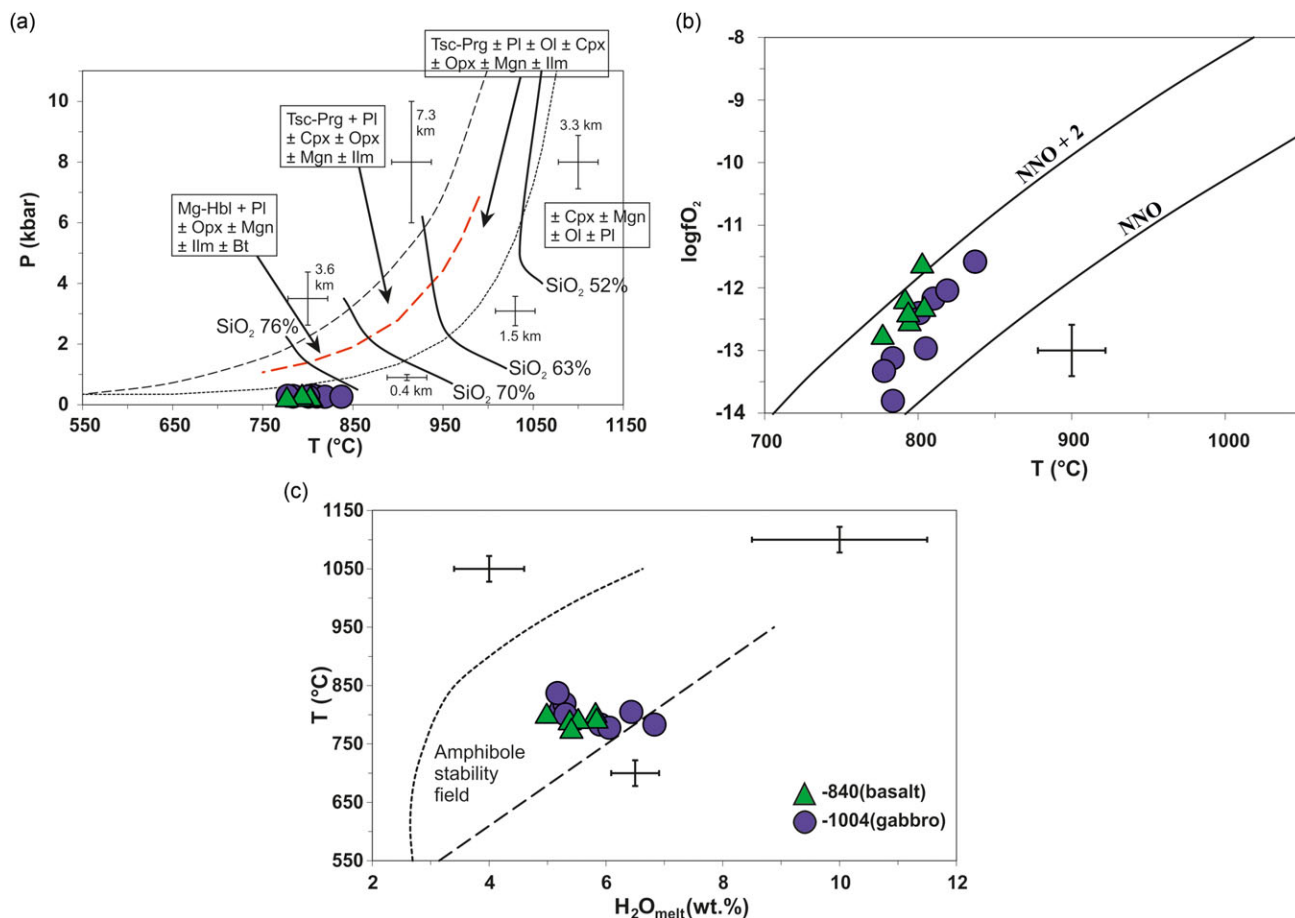
Fig. 7. (Colour online) (a) Amphibole compositional data in the thermobarometric field proposed by Ridolfi *et al.* (2010); (b) Amphibole composition for determination of oxygen fugacity; (c) Estimated H₂O melt compositions in a binary plot involving *T* (°C) and H₂O in the melt. For details see text and Ridolfi *et al.* (2010) (while plotting, only relevant compositions of amphibole were considered that qualify under the criteria).
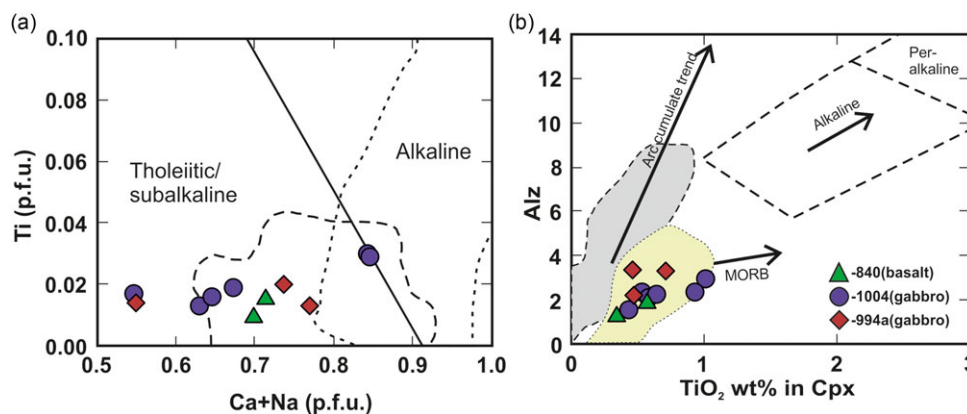

Fig. 8. (Colour online) Variation diagrams involving pyroxene compositions to constrain parental magma composition: (a) Ti (pfu) versus Ca + Na (pfu) (Leterrier *et al.* 1982); (b) Al$_z$ versus TiO₂ wt % (Loucks, 1990). Note: From (a) it is evident that the parent magma possesses a sub-alkaline/tholeiitic character whereas for (b), the data plots for the pyroxene stippled field defined a compositional array that is broadly following the arc cumulate trend (Loucks, 1990).

and, therefore, recognition of any relict minerals is very difficult (except for magnetite and chromite). It is possible that the supposed initial olivine was reacted upon and destabilized in a CO₂-rich environment (Olsson *et al.* 2012) and subsequently serpentinized to a great extent by the hydration event as discussed earlier (Berndt *et al.* 1996; D'Antonio & Kristensen, 2004; Lamadrid *et al.* 2017).

7.b. Quantitative evaluation of crystallization

Quantitative modelling of the crystallization history of the parent basic magma was undertaken using Petrolog3 software that involves algorithm calculations (Danyushevsky & Plechov, 2011). Using this software, an attempt has been made to understand mineral–melt equilibrium milieu (liquidus temperature) and the
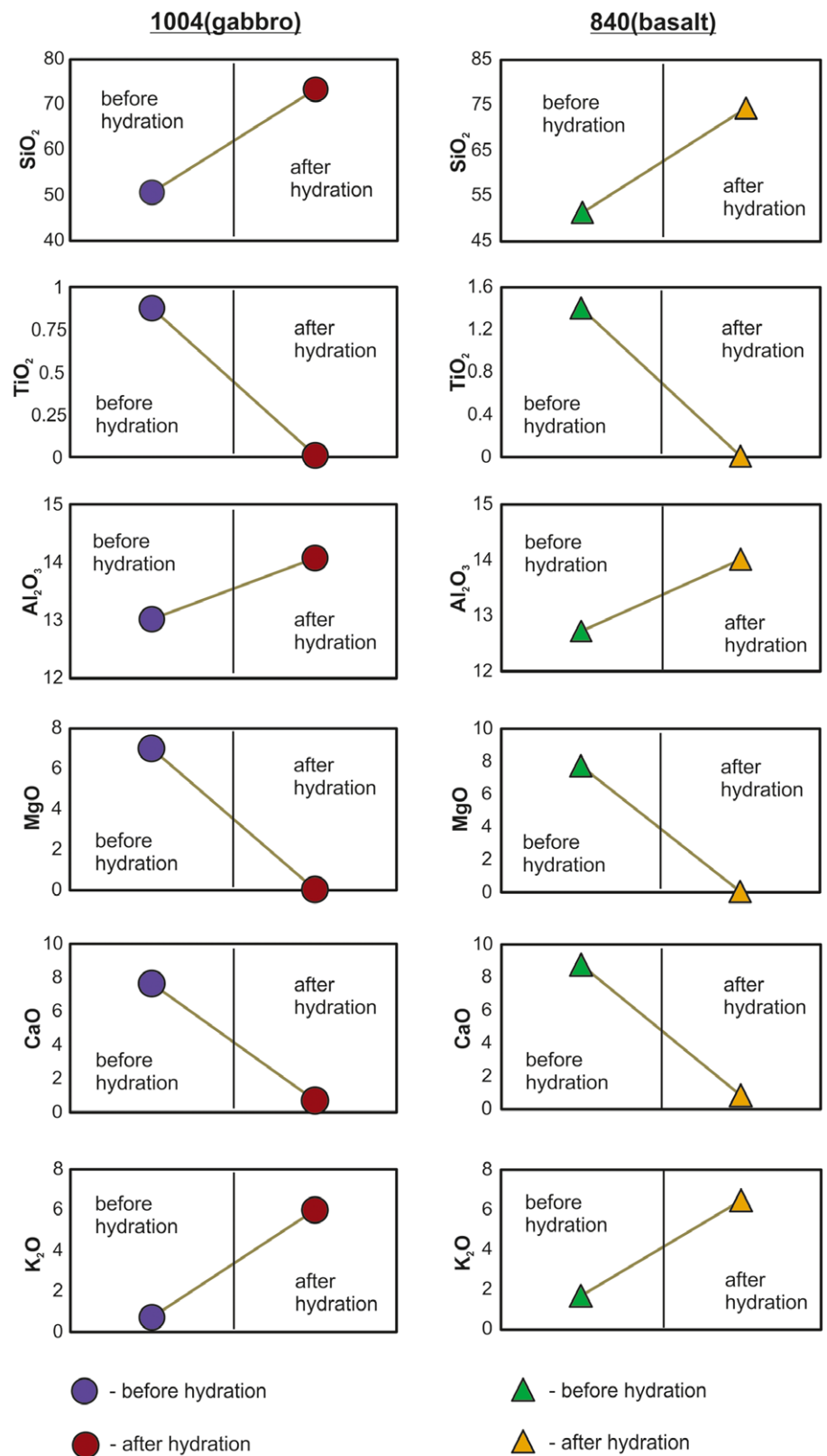
Fig. 9. (Colour online) Variation plots of several oxides before and after hydration of the magma. Oxide percentages before hydration were taken from M. Paul's (first author of this paper) unpublished data, whereas data after hydration were calculated using equations provided by Zhang *et al.* (2017). Left-hand panel for specimen no. 1004 (gabbro) and right-hand panel for specimen no. 840 (basalt). This diagram has been constructed to compare the compositional variation before and after hydration.

quantification of physical parameters such as density, viscosity and oxygen fugacity. The output data obtained from the Petrolog3 software are given in Table 4 and the evaluated liquidus temperatures are presented in Figure 10. It is evident from this figure that olivine ubiquitously represents the highest liquidus temperature. In the present case, the appearance of olivine in peridotite is quite expected (though overwhelmingly serpentinized), while both gabbro and basalt are devoid of olivine. It is possible that subsequent to olivine crystallization, it started reacting with the ambient liquid, leading to its complete disappearance. As a result of the olivine

Table 4. Various parameters related to the crystallization history of the investigated plutonic and volcanic lithologies using Petrolog3 software

Sr. no.	Rock type	Source composition (parent melt) (major element data in wt %)	% of fractional crystallization	Appearance of minerals with liquidus temperatures (°C)	Equilibration pressure (in kbar) based on data obtained from Putirka (2008)	Density of the parent melt (gm/cc)	Prevalent oxygen fugacity (fO_2)	Viscosity (in poise)
1	Basalt	SiO_2 – 52.00 TiO_2 – 1.36 Al_2O_3 – 12.99 Fe_2O_3 – 1.43 FeO – 9.77 MnO – 0.16 MgO – 8.92 CaO – 8.70 Na_2O – 3.06 K_2O – 1.44 P_2O_5 – 0.17	Olv – 5 Plag – 58 Cpx – 30 Pig – 1 Spl – 2 Ilm – 2 Mgt – 2	Olv (1255) Opx (1214) Pig (1209) Cpx (1200) Plag (1149) Spl (1091) Mgt (1060) Ilm (876)	0.001	2.66	−7.7	584
2	Gabbro	SiO_2 – 51.99 TiO_2 – 1.36 Al_2O_3 – 12.99 Fe_2O_3 – 1.52 FeO – 9.69 MnO – 0.16 MgO – 8.92 CaO – 8.69 Na_2O – 3.06 K_2O – 1.44 P_2O_5 – 0.17	Plag – 48 Cpx – 45 Ilm – 5 Mgt – 2	Olv (1286) Pig (1251) Opx (1214) Cpx (1200) Plag (1169) Spl (1091) Mgt (1060) Ilm (876)	6	2.65	−7.4	416
3	Gabbro	SiO_2 – 51.98 TiO_2 – 1.36 Al_2O_3 – 12.99 Fe_2O_3 – 1.73 FeO – 9.49 MnO – 0.16 MgO – 8.91 CaO – 8.69 Na_2O – 3.06 K_2O – 1.44 P_2O_5 – 0.17	Plag – 48 Cpx – 45 Ilm – 5 Mgt – 2	Olv (1363) Pig (1356) Plag (1225) Opx (1214) Cpx (1200) Spl (1091) Mgt (1060) Ilm (876)	21	2.64	−6.6	177
4	Ultramafic	SiO_2 – 51.98 TiO_2 – 1.36 Al_2O_3 – 12.99 Fe_2O_3 – 1.73 FeO – 9.49 MnO – 0.16 MgO – 8.91 CaO – 8.69 Na_2O – 3.06 K_2O – 1.44 P_2O_5 – 0.17	Olv – 40 Opx – 50 Cpx – 5 Spl – 3 Mgt – 2	Olv (1363) Pig (1356) Plag (1225) Opx (1214) Cpx (1200) Spl (1091) Mgt (1060) Ilm (876)	21	2.64	−6.6	177
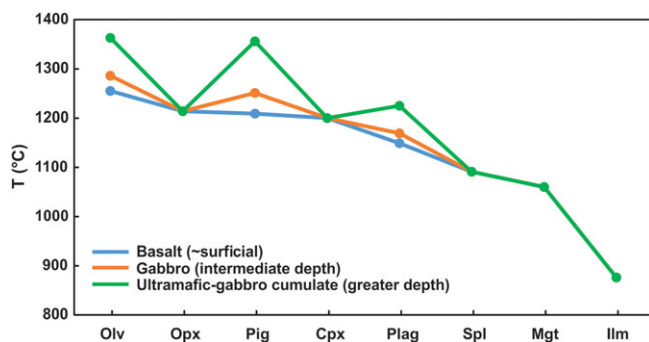
Fig. 10. (Colour online) Output of Petrolog3 data showing calculated liquidus temperatures (in °C) for different constituent minerals for the mafic–ultramafic rock suites.

and liquid reaction during equilibrium crystallization, augitic clinopyroxene became the stable mineral phase. In addition to equilibrium crystallization, fractional crystallization also played an important role, which has been supported by textural evidence. Back-scattered electron images (Fig. 4b, c) clearly indicate the presence of clinopyroxene and zoned plagioclase phenocrysts set in a fine-grained groundmass in some basaltic samples, favouring fractional crystallization. Therefore, the parent magma represents a combination of both equilibrium and fractional crystallization, which is an expected behaviour in a realistic situation for crystallization of the basaltic magma (Morse, 1980). Furthermore, the Petrolog3 software suggests an almost constant magma density (~2.6 gm/cc) with the onset of crystallization (Table 4). The oxygen fugacity (during the magma ascent) changes from −7.7 to −6.6. The reason for such a variation needs clarification. The progressive
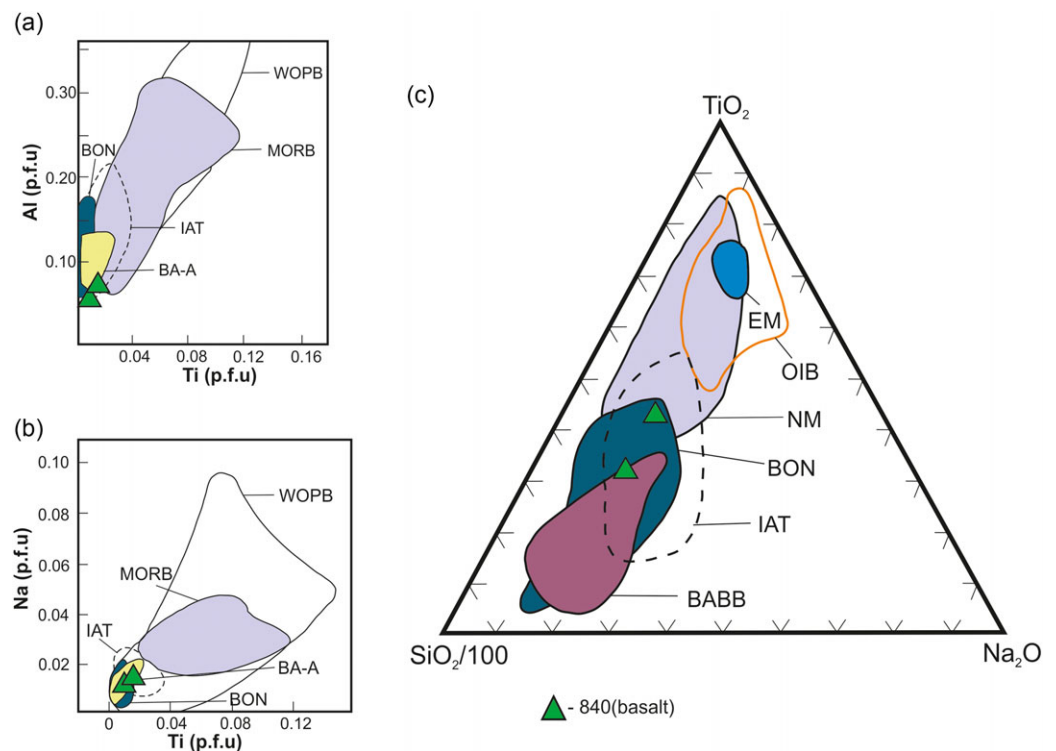
Fig. 11. (Colour online) Tectonic discrimination diagrams using pyroxene composition: (a) Al (pfu) versus Ti (pfu) diagram; (b) Na (pfu) versus Ti (pfu) diagram; (c) TiO_2–SiO_2/100–Na_2O diagram (Beccaluva *et al.* 1989; Ovung *et al.* 2018). All these diagrams suggest an overall island arc tectonic setting. WOPB – within oceanic plate basalts; MORB – mid-ocean ridge basalts; IAT – island arc tholeiites; BA-A – back-arc andesites; BON – boninites; EM – enriched mid-ocean ridge basalts; NM – normal mid-ocean ridge basalts; OIB – ocean island basalts; BABB – back-arc basin basalts.

reduction of oxygen fugacity from the bottom to the top of the magma chamber may be ascribed to heating and reduction during magma ascent. Anderson & Wright (1972) suggested controversially that during the onset of magma eruption, it effervesces and suffers a reducing environment because of (i) loss of H_2O, (ii) loss of SO_2 and (iii) probable magma mixing. Magma effervescence during ascent is found to be a definite cause of accelerated crystallization of micro-phenocrysts, a rise in temperature and a decrease in oxidation state. The Petrolog3 software also yields liquidus temperatures (in respect of several minerals) for the investigated basaltic–mafic–ultramafic rock suites (Fig. 10). This figure suggests the possible presence of initial pigeonite for both the basalt and gabbro, but in the investigated samples, pigeonite has not been noted. Interestingly, for the ultramafic, gabbro and basaltic samples, oxide phases (such as spinel, magnetite and ilmenite) have similar liquidus temperatures (1091–876 °C) (Fig. 10; Table 4), which indicates that the oxide phases have a uniform late-phase appearance. Therefore, we conclude that the parent magma evolved through a complex history involving the interplay of repeated pulses of magma ascent, fluctuation of the crystallization condition, effervescence and possibly localized scale magma mixing.

7.c. Evaluation of the tectonic setting

The evaluation of the tectonic setting for these rocks can be achieved using mineral chemistry. Given the mineralogical assemblages, clinopyroxene and spinel were considered to be the most appropriate. The petrogenesis and tectonic lineage of basaltic rocks have been derived from EPMA of augitic clinopyroxene (Beccaluva *et al.* 1989). This approach has been subsequently taken up by other workers to evaluate the status of the Manipur Ophiolite suite of rocks (Ovung *et al.* 2018). EPMA data for the clinopyroxene compositions (online Supplementary Material Table S1) when plotted on an Al (pfu) versus Ti (pfu) diagram (Fig. 11a) typically

suggest an island arc tholeiitic (IAT) affinity. Similar IAT parentage is indicated by the Na (pfu) versus Ti (pfu) diagram (Fig. 11b). Figure 11c represents a triangular diagram involving TiO_2–SiO_2/100–Na_2O, which also suggests an IAT affinity for the basaltic rocks.

Spinel chemistry can be used to discriminate the tectonic setting of various types of rocks (Dick & Bullen, 1984; Jan & Windley, 1990; Arai, 1992; Hirose & Kawamoto, 1995; Kamenetsky *et al.* 2001; Ovung *et al.* 2017; Ishwar-Kumar *et al.* 2018; Sahu *et al.* 2020). In the present case, the available spinel compositions of the ultramafic rocks (online Supplementary Material Table S5), using the TiO_2 (wt %) versus Al_2O_3 (wt %) diagram (Fig. 12a), typically indicate an arc affinity for the parent magma. A similar (island) arc affinity can also be derived from the TiO_2 (wt %) versus Cr/(Cr + Al) diagram (Fig. 12b). Figure 12c involving Cr no. in spinel versus Mg no. in spinel further corroborates the tectonic setting to be akin to fore-arc peridotite. A boninitic magma chemistry (related to an arc setting) can further be derived from the Cr no. in (Spl) versus TiO_2 (wt %) (Spl) diagram (Fig. 12d).

### 8. Conclusions

The following conclusions can be drawn regarding the petrogenesis of the studied rock units:

(1) The Palaeoarchaean mafic–ultramafic rock suite shows a varied temperature–pressure equilibration, ranging from ~750 °C to ~1400 °C at ~0.26 kbar to ~21 kbar, which corresponds to an ascending magma that underwent a hydration event at a shallow level (Fig. 13).
(2) The clinopyroxene and spinel compositions indicate an arc setting for the parent magma.
(3) Both equilibrium and fractional crystallization prevailed during the magmatic evolution.
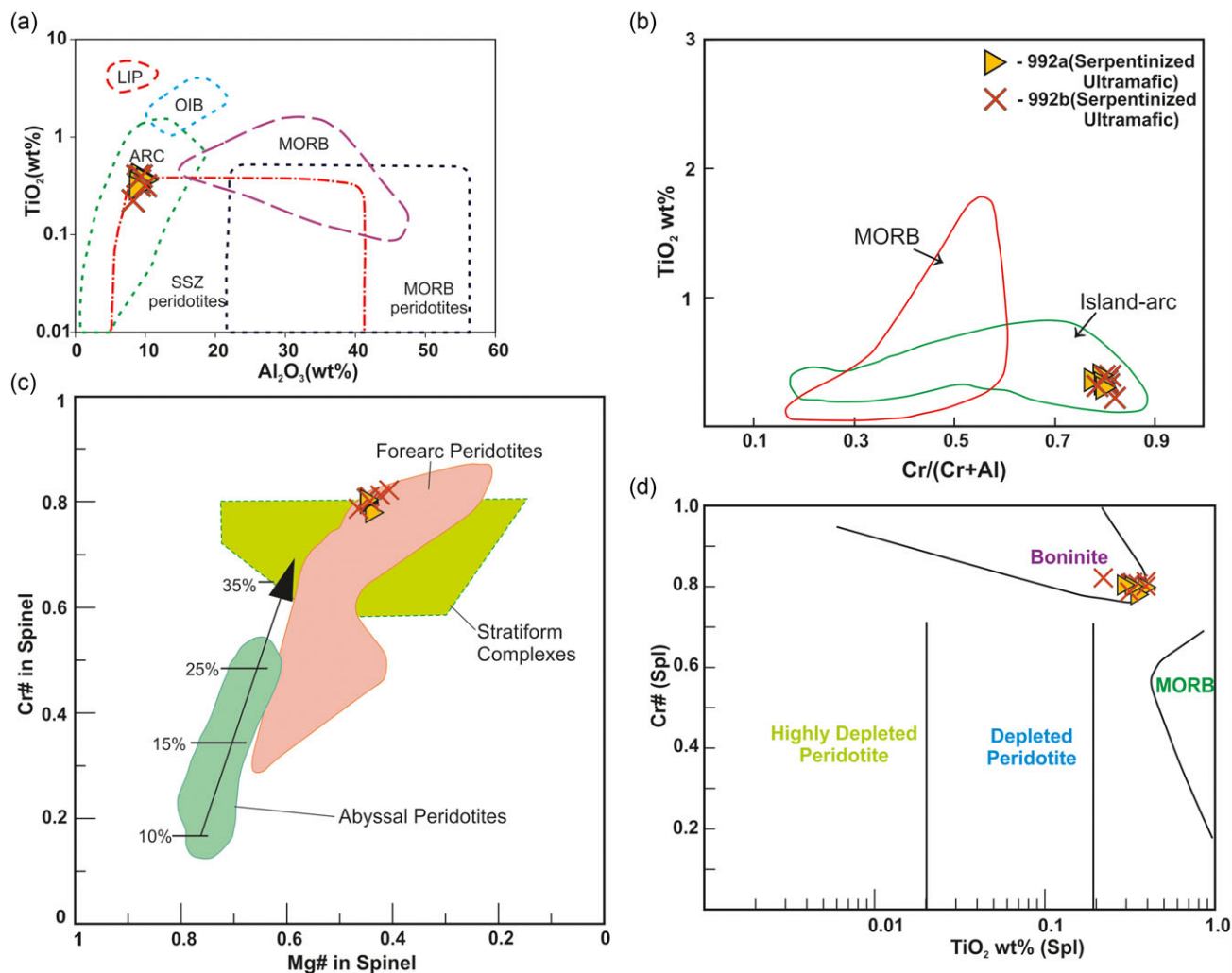
Fig. 12. (Colour online) Tectonic discrimination diagrams using Cr-spinel composition: (a) TiO_2 wt % versus Al_2O_3 wt %; (b) TiO_2 wt % versus $Cr/(Cr+Al)$; (c) Cr no. versus Mg no.; (d) Cr no. versus TiO_2 wt %. All these diagrams clearly suggest an island arc/boninite/fore-arc peridotite affinity relevant to the supra-subduction zone setting. For details see text and Dick & Bullen (1984), Jan & Windley (1990), Arai (1992), Ishii *et al.* (1992), Hirose & Kawamoto (1995), Kamenetsky *et al.* (2001), Ovung *et al.* (2017) and Sahu *et al.* (2020). ARC – island arc; LIP – large igneous province; OIB – ocean island basalt; MORB – mid-ocean ridge basalt; SSZ – supra-subduction zone.
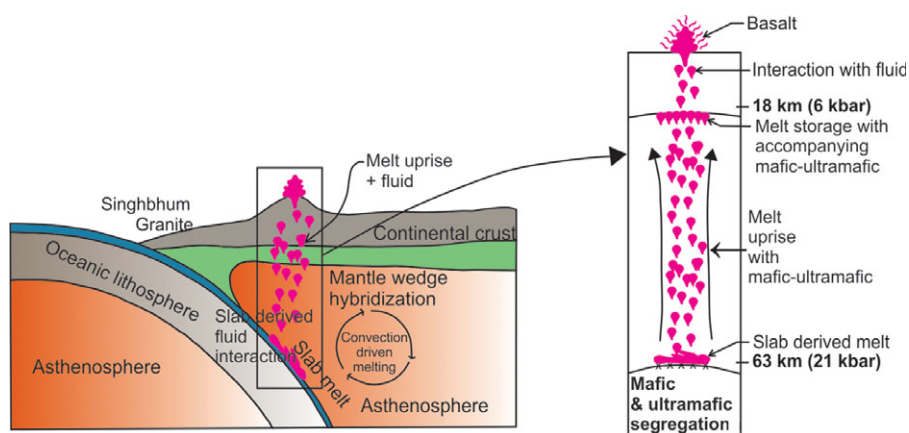
Fig. 13. (Colour online) Schematic diagram showing summary of evolution of mafic–ultramafic rock suites in the investigated areas in the light of the regional framework.

References

Abdelfadil KM, Saleh GM, Putiš M and Sami M (2022) Mantle source characteristics of the late Neoproterozoic post-collisional gabbroic intrusion of Wadi Abu Hadieda, north Arabian-Nubian Shield, Egypt. *Journal of African Earth Sciences* **194**, 104607. doi: 10.1016/j.jafrearsci.2022.104607.

Acharyya S, Gupta A and Orihashi Y (2010) Neoarchean–Paleoproterozoic stratigraphy of the Dhanjori basin, Singhbhum Craton, Eastern India: and recording of a few U–Pb zircon dates from its basal part. *Journal of Asian Earth Sciences* **39**, 527–36.

Adhikari A, Nandi A, Mukherjee S and Vadlamani R (2021) Petrogenesis of Neoarchean (2.80–2.75 Ga) Jagannathpur volcanics and the Ghatgaon and Keshargaria dyke swarms, Singhbhum craton, eastern India: geochemical, Sr-Nd isotopic and Sm-Nd geochronologic constraints for interaction of enriched-DMM derived magma with metasomatized subcontinental lithospheric mantle. *Lithos* **400–401**, 106373. doi: 10.1016/j.lithos.2021.106373.

Adhikari A and Vadlamani R (2022) Petrogenesis of the Mesoarchean (~3.05 Ga) mafic volcanics from the western Iron Ore Group volcano-sedimentary succession, Singhbhum craton, eastern India: constraints from geochemical modelling and Sm-Nd geochronology. *Lithos* **412–413**, 106596. doi: 10.1016/j.lithos.2022.106596.

Ali S, Ntaflos T and Sami M (2021) Geochemistry of Khor Um-Safi ophiolitic serpentinites, central Eastern Desert, Egypt: implications for Neoproterozoic arc-basin system in the Arabian-Nubian shield. *Geochemistry* **81**, 125690. doi: 10.1016/j.chemer.2020.125690.

Anderson AT and Wright TL (1972) Phenocrysts and glass inclusions and their bearing on oxidation and mixing of basaltic magmas, Kilauea volcano, Hawaii. *American Mineralogist* **57**, 188–216.

Arai S (1992) Chemistry of chromian spinel in volcanic rocks as a potential guide to magma chemistry. *Mineralogical Magazine* **56**, 173–84.

Barnes SJ and Roeder PL (2001) The range of spinel compositions in terrestrial mafic and ultramafic rocks. *Journal of Petrology* **42**, 2279–302.

Basu AR, Bandyopadhyay PK, Chakraborti R and Zou H (2008) Large 3.4 Ga Algoma type BIF in the Eastern Indian Craton. *Goldschmidt Conference Abstracts. Geochimica et Cosmochimica Acta* **72**, A59.

Beccaluva L, Macciotta G, Piccardo GB and Zeda O (1989) Clinopyroxene composition of ophiolite basalts as petrogenetic indicator. *Chemical Geology* **77**, 165–82.

Berndt ME, Allen DE and Seyfried WE Jr (1996) Reduction of CO_2 during serpentinization of olivine at 300°C and 500 bar. *Geology* **24**, 351–4.

Bhattacharjee S, Mulder JA, Roy S, Chowdhury P, Cawood PA and Nebel O (2021) Unravelling depositional setting, age and provenance of the Simlipal volcano-sedimentary complex, Singhbhum craton: evidence for Hadean crust and Mesoarchean marginal marine sedimentation. *Precambrian Research* **354**, 106038. doi: 10.1016/j.precamres.2020.106038.

Byerly GR and Lowe DR (2014) Paleoarchean ocean crust and mantle excavated by meteor impact: insight into early crustal processes and tectonics. *Geology* **42**, 635–8.

Chakraborti TM, Ray A, Deb GK, Upadhyay D and Chakrabarti R (2019) Evidence of crustal reworking in the Mesoarchean: insights from geochemical, U–Pb zircon and Nd isotopic study of a 3.08–3.12 Ga ferro-potassic granite gneiss from north-eastern margin of Singhbhum Craton, India. *Lithos* **330–331**, 16–34.

Chaudhuri T, Wan Y, Mazumder R, Ma M and Liu D (2018) Evidence of enriched, Hadean mantle reservoir from 4.2–4.0 Ga zircon xenocrysts from Paleoarchean TTGs of the Singhbhum Craton, Eastern India. *Scientific Reports* **8**, 7069. doi: 10.1038/s41598-018-25494-6.

D'Antonio M and Kristensen MB (2004) Serpentine and brucite of ultramafic clasts from the South Chamorro Seamount (Ocean Drilling Program Leg 196, Site1200): inferences for the serpentinization of the Mariana forearc mantle. *Mining Magazine* **68**, 887–904.

Danyushevsky LV and Plechov P (2011) Petrolog3: integrated software for modeling crystallization processes. *Geochemistry, Geophysics, Geosystems* **12**, Q07021. doi: 10.1029/2011GC003516.

Das S, Goswami B and Bhattacharyya C (2020) Physico-chemical conditions of crystallization and composition of source magma of the Grenvillian post-collisional mafic-ultramafic rocks in the Chhotanagpur Gneissic Complex, Eastern India. *Journal of Earth System Science* **129**, 89. doi: 10.1007/s12040-019-1313-4.

Deer WA, Howie RA and Zussman J (1992) *An Introduction to the Rock-Forming Minerals* (2nd edition). Harlow: Longman Scientific and Technical, 696 pp.

Dick HJB and Bullen T (1984) Cr-spinel as a petrogenetic indicator in abyssal and alpine-type peridotites and spatially associated lavas. *Contributions to Mineralogy and Petrology* **86**, 54–76.

Friend CRL, Bennett VC and Nutman AP (2002) Abyssal peridotites >3,800 Ma from southern West Greenland: field relationships, petrography, geochronology, whole-rock and mineral chemistry of dunite and harzburgite inclusions in the Itsaq Gneiss Complex. *Contributions to Mineralogy and Petrology* **143**, 71–92.

Gillis KM (1995) Controls on hydrothermal alteration in a section of fast-spreading oceanic crust. *Earth and Planetary Science Letters* **134**, 473–89.

Guice GL, McDonald I, Hughes HSR, MacDonald JM, Blenkinsop TG, Goodenough KM, Faithfull JW and Gooday RJ (2018) Re-evaluating ambiguous age relationships in Archean cratons: implications for the origin of ultramafic-mafic complexes in the Lewisian Gneiss Complex. *Precambrian Research* **311**, 136–56.

Hawthorne FC, Oberti R, Harlow GE, Maresch WV, Martin RF, Schumacher JC and Welch MD (2012) IMA report: nomenclature of the amphibole supergroup. *American Mineralogist* **97**, 2031–48.

Hey MH (1954) A new review of the chlorites. *Mineralogical Magazine and Journal of the Mineralogical Society* **30**, 277–92.

Hirose K and Kawamoto T (1995) Hydrous partial melting of lherzolite at 1 GPa: the effect of H_2O on the genesis of basaltic magmas. *Earth and Planetary Science Letters* **133**, 463–73.

Hofmann A, Jodder J, Xie H, Bolhar R, Whitehouse M and Elburg M (2022) The Archaean geological history of the Singhbhum Craton, India – a proposal for a consistent framework of craton evolution. *Earth-Science Reviews* **228**, 103994. doi: 10.1016/j.earscirev.2022.103994.

Hövelmann J, Putnis A, Geisler T, Schmidt BC and Golla-Schindler U (2010) The replacement of plagioclase feldspars by albite: observations from hydrothermal experiments. *Contributions to Mineralogy and Petrology* **159**, 43–59.

Humphris SE and Thompson G (1978) Hydrothermal alteration of oceanic basalts by seawater. *Geochimica et Cosmochimica Acta* **42**, 107–25.

Ishii T, Robinson PT, Maekawa H and Fiske R (1992) Petrological studies of peridotites from diapiric serpentinite seamounts in the Izu-Ogasawara-Mariana forearc, Leg 125. *In Proceedings of the Ocean Drilling Program, Scientific Results, vol. 125* (eds P Fryer, JA Pearce, LB Stokking, JR Ali, R Arculus, D Ballotti, MM Burke, G Ciampo, JA Haggerty, RB Haston, D Heling, MA Hobart, T Ishii, LE Johnson, Y Lagabrielle, FW McCoy, H Maekawa, MS Marlow, G Milner, MJ Mottl, BJ Murton, SP Phipps, CA Rigsby, KL Saboda, B Stabell, S van der Lann and Y Xu), pp. 445–85. College Station, Texas.

Ishwar-Kumar C, Rajesh VJ, Windley BF, Razakamanana T, Itaya T, Babu EVSSK and Sajeev K (2018) Chromite chemistry as an indicator of petrogenesis and tectonic setting of the Ranomena ultramafic complex in north-eastern Madagascar. *Geological Magazine* **155**, 109–18.

Jan MQ and Windley BF (1990) Chromian spinel-silicate chemistry in ultramafic rocks of the Jijal complex, Northwest Pakistan. *Journal of Petrology* **31**, 667–715.

Jayananda M, Kano T, Peucat JJ and Channabasappa S (2008) 3.35 Ga komatiite volcanism in the western Dharwar craton, southern India: constraints from Nd isotopes and whole-rock geochemistry. *Precambrian Research* **162**, 160–79.

Kamenetsky VS, Crawford AJ and Meffre S (2001) Factors controlling chemistry of magmatic spinel: an empirical study of associated olivine, Cr-spinel and melt inclusions from primitive rocks. *Journal of Petrology* **42**, 655–71.

Lamadrid HM, Rimstidt JD, Schwarzenbach EM, Klein F, Ulrich S, Dolocan A and Bodnar RJ (2017) Effect of water activity on rates of serpentinization of olivine. *Nature Communications* **8**, 16107. doi: 10.1038/ncomms16107.

Leake BE (1978) Nomenclature of amphiboles. *Mineralogical Magazine* **42**, 533–63.

Leake BE, Woolley AR, Arps CES, Birch WD, Gilbert MC, Grice JD, Hawthorne FC, Kato A, Kisch HJ, Krivovichev VG, Linthout K, Laird J, Mandarino J, Maresch WV, Nickel EH, Rock NMS, Schumacher JC, Smith DC, Stephenson NCN, Ungaretti L, Whittaker EJW and Youzhi G (1997) Nomenclature of amphiboles: report of the Subcommittee on Amphiboles of the International Mineralogical Association, Commission on New Minerals and Mineral Names. *Canadian Mineralogist* **35**, 219–46.

Leterrier J, Maury RC, Thonon P, Girard D and Marchal M (1982) Clinopyroxene composition as a method of identification of the magmatic affinities of paleo-volcanic series. *Earth and Planetary Science Letters* **59**, 139–54.

Li ZX, Bogdanova SV, Collins AS, Davidson A, De Waele B, Ernst RE, Fitzsimons ICW, Fuck RA, Gladkochub DP, Jacobs J, Karlstrom KE, Lu S, Natapov LM, Pease V, Pisarevsky SA, Thrane K and Vernikovsky V (2008) Assembly, configuration, and break-up history of Rodinia: a synthesis. *Precambrian Research* **160**, 179–210.

Loucks RR (1990) Discrimination of ophiolitic from nonophiolitic ultramafic–mafic allochthons in orogenic belts by the Al/Ti ratio in clinopyroxene. *Geology* **18**, 346–9.

Mahapatra RR, Mukherjee P, Paul M, Chakraborti S, Ray J, Ganguly S, Koeberl C, Manikyamba C and Sarkar S (2022) Style of fractional crystallization in basalts from the Paleoarchean western Iron Ore Group of Singhbhum Craton, Eastern India: implications from one atmosphere experimental studies. *Journal of the Geological Society of India* **98**, 627–34.

Malviya VP, Arima M, Pati JK and Kaneko Y (2006) Petrology and geochemistry of metamorphosed basaltic pillow lava and basaltic komatiite in the Mauranipur area: subduction related volcanism in the Archean Bundelkhand craton, Central India. *Journal of Mineralogical and Petrological Sciences* **101**, 199–217.

Marti S, Stünitz H, Heilbronner R, Plümper O and Kilian R (2018) Syn-kinematic hydration reactions, grain size reduction, and dissolution-precipitation creep in experimentally deformed plagioclase-pyroxene mixtures. *Solid Earth* **9**, 985–1009.

Matin A, Banerjee S, Gupta CD and Banerjee N (2012) Progressive deformation across a ductile shear zone: an example from the Singhbhum Shear Zone, eastern India. *International Geology Review* **54**, 290–301.

Meert JG, Pandit MK, Pradhan VR, Banks J, Sirianni R, Stroud M, Newstead B and Gifford J (2010) Precambrian crustal evolution of peninsular India: a 3.0 billion year odyssey. *Journal of Asian Earth Sciences* **39**, 483–515.

Misra S (2006) Precambrian chronostratigraphic growth of Singhbhum Orissa Craton, Eastern Indian shield: an alternative model. *Journal of Geological Society of India* **67**, 356–78.

Misra S, Deomurari MP, Wiedenbeck M, Goswami JN, Ray SL and Saha AK (1999) $^{207}Pb/^{206}Pb$ zircon ages and the evolution of the Singhbhum Craton, eastern India: an ion microprobe study. *Precambrian Research* **93**, 139–51.

Morimoto N (1989) Nomenclature of pyroxenes. *Canadian Mineralogist* **27**, 143–56.

Morimoto N, Fabries J, Ferguson AK, Ginzburg IV, Ross M, Seifert FA, Zussman J, Aoki K and Gottardi G (1988) Nomenclature of pyroxenes. *American Mineralogist* **73**, 1123–33.

Morse SA (1980) *Basalts and Phase Diagrams: An Introduction to the Quantitative Use of Phase Diagrams in Igneous Petrology*. New York: Springer Verlag, 493 pp.

Mukhopadhyay D (2001) The Archean nucleus of Singhbhum: the present state of knowledge. *Gondwana Research* **4**, 307–18.

Mukhopadhyay J, Beukes NJ, Armstrong RA, Zimmermann U, Ghosh G and Medda RA (2008) Dating the oldest greenstone in India: a 3.51 Ga precise U–Pb SHRIMP Zircon age for dacitic lava of the Southern Iron Ore Group, Singhbhum Craton. *Journal of Geology* **116**, 449–61.

Mukhopadhyay D and Matin A (2020) The architecture and evolution of the Singhbhum Craton. *Episodes* **43**, 19–50.

Nelson DR, Bhattacharya H, Thern ER and Altermann W (2014) Geochemical and ion-microprobe U–Pb zircon constraints on the Archaean evolution of Singhbhum Craton, eastern India. *Precambrian Research* **255**, 412–32.

Olierook HKH, Clark C, Reddy SM, Mazumder R, Jourdan F and Evans NJ (2019) Evolution of the Singhbhum Craton and supracrustals provinces from age, isotopic and chemical constraints. *Earth-Science Reviews* **193**, 237–59.

Olsson J, Bovet N, Makovicky E, Bechgaard K, Balogh Z and Stipp SLS (2012) Olivine reactivity with CO_2 and H_2O on a microscale: implications for carbon sequestration. *Geochimica et Cosmochimica Acta* **77**, 86–97.

O'Neill HSC (1981) The transition between spinel lherzolite and garnet lherzolite, and its use as a geobarometer. *Contributions to Mineralogy and Petrology* **77**, 185–94.

Ovung TN, Ray J, Ghosh B, Koeberl C, Topa D and Paul M (2018) Clinopyroxene composition of volcanics from the Manipur Ophiolite, Northeastern India: implications to geodynamic setting. *International Journal of Earth Sciences* **107**, 1215–29.

Ovung TN, Ray J, Teng X, Ghosh B, Paul M, Ganguly P, Sengupta S and Das S (2017) Mineralogy of the Manipur Ophiolite Belt, North East India: implications for mid-oceanic ridge and supra-subduction zone origin. *Current Science* **112**, 2122–9.

Paul M, Ray J, Manikyamba C, Ganguly S, Singh MR, Pachal S and Sarkar D (2021) Mafic volcanic rocks of western Iron Ore Group, Singhbhum craton, eastern India: geochemical evidence for ocean-continent convergence. *Geological Journal* **56**, 102–29. doi: 10.1002/gj.3944.

Pettigrew NT and Hattori KH (2006) The Quetico Intrusions of Western Superior Province: neo-Archean examples of Alaskan/Ural-type mafic-ultramafic intrusions. *Precambrian Research* **149**, 21–42.

Polat A and Hofmann AW (2003) Alteration and geochemical patterns in the 3.7–3.8 Ga Isua greenstone belt, West Greenland. *Precambrian Research* **126**, 197–218.

Putirka K (2008) Thermometers and barometers for volcanic systems. *Reviews in Mineralogy and Geochemistry* **69**, 61–120.

Radhakrishna BP and Naqvi SM (1986) Precambrian continental crust of India and its evolution. *Journal of Geology* **94**, 145–66.

Ramakrishnan M and Vaidyanadhan R (2008) *Geology of India: Volume 1*. Bangalore: Geological Society of India, 556 pp.

Ridolfi F and Renzulli A (2012) Calcic amphiboles in calc-alkaline and alkaline magmas: thermobarometric and chemometric empirical equations valid up to 1,130°C and 2.2 GPa. *Contributions to Mineralogy and Petrology* **163**, 877–95.

Ridolfi F, Renzulli A and Puerini M (2010) Stability and chemical equilibrium of amphibole in calc-alkaline magmas: an overview, new thermobarometric formulations and application to subduction-related volcanoes. *Contributions to Mineralogy and Petrology* **160**, 45–66.

Rogers JJW and Santosh M (2002) Configuration of Columbia, a Mesoproterozoic supercontinent. *Gondwana Research* **5**, 5–22.

Saha AK (1994) *Crustal Evolution of Singhbhum-North Orissa, Eastern India*. Geological Society of India, Memoir no. 27, 341 pp.

Saha AK, Ray SL and Sarkar SN (1988) Early history of the Earth: evidence from the Eastern Indian shield. In *Precambrian of the Eastern Indian Shield* (ed. D Mukhopadhyay), pp. 13–37. Geological Society of India, Memoir no. 8.

Sahu A, Vishwakarma N, Singh Y and Verma CB (2020) Mineral chemistry of high-Al chromian spinel from ultramafic rocks of the Babina-Prithvipur

transect, Bundelkhand Craton, central India: implications for petrogenesis and tectonic setting. *Journal of Earth System Science* **129**, 1–19. doi: 10.1007/s12040-020-01448-3.

Sarkar SC and Gupta A (2012) *Crustal Evolution and Metallogeny in India.* Cambridge: Cambridge University Press, 840 pp.

Schmädicke E (2000) Phase relations in peridotitic rocks in the model system CMASH and NCMASH. *Journal of Petrology* **41**, 69–86.

Sharma RS (2009) *Cratons and Fold Belts of India*. Heidelberg: Springer Verlag, 322 pp.

Singh MR, Manikyamba C, Ray J, Ganguly S, Santosh M, Saha A, Rambabu S and Sawant SS (2016) Major, trace and platinum group element (PGE) geochemistry of Archean Iron Ore Group and Proterozoic Malangtoli metavolcanics rocks of Singhbhum Craton, Eastern India: inferences on mantle melting and sulphur saturation history. *Ore Geology Reviews* **72**, 1263–89.

Sreenivas B, Dey S, Bhaskar Rao YJ, Vijaya Kumar T, Babu EVSSK and Williams IS (2019) A new cache of Eoarchaean detrital zircons from the Singhbhum Craton, eastern India and constraints on early Earth geodynamics. *Geoscience Frontiers* **10**, 1359–70.

Srivastava RK, Söderlund U, Ernst RE, Mondal SK and Samal AK (2019) Precambrian mafic dyke swarms in the Singhbhum craton (eastern India) and their links with dyke swarms of the eastern Dharwar craton (southern India). *Precambrian Research* **329**, 5–17.

Stakes D and Vanko DA (1986) Multistage hydrothermal alteration of gabbroic rocks from the failed Mathematician Ridge. *Earth and Planetary Science Letters* **79**, 75–92.

Stevens RE (1944) Composition of some chromites of the western hemisphere. *American Mineralogist* **29**, 1–34.

Stünitz H and Tullis J (2001) Weakening and strain localization produced by syn-deformational reaction of plagioclase. *International Journal of Earth Sciences* **90**, 136–48.

Upadhyay D, Chattopadhyay S, Kooijman E, Mezger K and Berndt J (2014) Magmatic and metamorphic history of Paleoarchean tonalite–trondhjemite–granodiorite (TTG) suite from the Singhbhum craton, eastern India. *Precambrian Research* **252**, 180–90.

Veevers JJ (2004) Gondwanaland from 650–500 Ma assembly through 320 Ma merger in Pangea to 185–100 Ma breakup: supercontinental tectonics via stratigraphy and radiometric dating. *Earth-Science Reviews* **68**, 1–132.

Villanova-de-Benavent C, Proenza JA, Gali S, Casco AG, Tauler E, Lewis JF and Longo F (2014) Garnierites and garnierites: textures, mineralogy and geochemistry of garnierites in the Falcondo Ni-laterite deposit, Dominican Republic. *Ore Geology Reviews* **58**, 91–109.

Zhang J, Humphreys MCS, Cooper GF, Davidson JP and Macpherson CG (2017) Magma mush chemistry at subduction zones, revealed by new melt major element inversion from calcic amphiboles. *American Mineralogist* **102**, 1353–67.